40. Shimato, S.; Natsume, A.; Takeuchi, H.; Wakabayashi, T.; Fujii, M.; Ito, M.; Ito, S.; Park, I. H.; Bang, J. H.; Kim, S. U.; Yoshida, J. Human neural stem cells target and deliver therapeutic gene to experimental leptomeningeal medulloblastoma. Gene Ther. 14: 1132-1142; 2007.

41. Stejskal, E.; Tanner, J. Spin Diffusion Measurements: Spin Echoes in the Presence of a Time-Dependent Field Gradient. J. Chem. Phys. 42: 288-292; 1965.

42. Stichel, C. C.; Muller, H. W. The CNS lesion scar: new vistas on an old regeneration barrier. Cell Tissue Res. 294: 1-9; 1998.

43. Suzuki, H.; Fukuyama, R.; Hasegawa, Y.; Tamaki, T.; Nishio, M.; Nakashima, T.; Tatematsu, M. Tumor thickness, depth of invasion, and Bcl-2 expression are correlated with FDG-uptake in oral squamous cell carcinomas. Oral Oncol. 45: 891-897; 2009.

44. Takeuchi, H.; Natsume, A.; Wakabayashi, T.; Aoshima, C.; Shimato, S.; Ito, M.; Ishii, J.; Maeda, Y.; Hara, M.; Kim, S. U.; Yoshida, J. Intravenously transplanted human neural stem cells migrate to the injured spinal cord in adult mice in an SDF-1- and HGF-dependent manner. Neurosci. Lett. 426: 69-74; 2007.

45. Tang, B. L.; Low, C. B. Genetic manipulation of neural stem cells for transplantation into the injured spinal cord. Cell Mol. Neurobiol. 27: 75-85; 2007.

46. Tuszynski, M. H.; Grill, R.; Jones, L. L.; McKay, H. M.; Blesch, A. Spontaneous and augmented growth of axons in the primate spinal cord: effects of local injury and nerve growth factor-secreting cell grafts. J. Comp. Neurol. 449: 88-101; 2002.

47. Yasuhara, T.; Matsukawa, N.; Hara, K.; Yu, G.; Xu, L.; Maki, M.; Kim, S. U.; Borlongan CV Transplantation of human neural stem cells exerts neuroprotection in a rat model of Parkinson's disease. J. Neurosci. 26: 12497-12511; 2006.

48. Zella, D.; Romerio, F.; Curreli, S.; Secchiero, P.; Cicala, C.; Zagury, D.; Gallo, R. C. IFN-alpha 2b reduces IL-2 production and IL-2 receptor function in primary CD4+ T cells. J. Immunol. 164: 2296-2302; 2000.

**Figure legends**

**Figure 1.** (A) Significantly activated pathways at glial scar following spinal cord injury. (B) Toll-like receptor-4 is markedly upregulated in the lesioned astrocytes. pAS, primary cultured astrocytes; nSC, normal spinal cord; SCI-glia, glial scar in spinal cord injury.

**Figure 2.** F3 human neural stem cells migrate to mouse spinal cord injury (SCI) lesion site. (A) A hematoxilin and eosin stained section shows that a large number of transplanted neural stem cells infiltrated in the lesioned site. (B) Fluorescence microscopy reveals a large number of DiI-labeled F3 cells at the lesion site. (C) Immunohistochemical staining with anti-β-galactosidase (β-gal) antibody demonstrates that β-gal-positive cells are extensively distributed in the lesioned area of a mouse injected with F3 cells expressing β-gal (F3.LacZ). (D) Higher magnification of panel C. (E) A control injured animal injected with PBS alone; none of β-gal-positive cells are observed in the spinal cord. (F) Higher magnification of panel E. (G) IFN-β mRNA expression is detected at the SCI site of the animals injected with F3.CD.IFN-β neural stem cells by RT-PCR. F3.CD.IFN:positive control; SCI/F3.CD.IFN: SCI site of an animal injected with F3.CD.IFN-β cells; SCI, SCI site of an animal injected with PBS only.



**Figure 3.** F3.CD.IFN-β cells inhibit growth of primary normal astrocytes. Astrocytes were co-cultured with either F3.LacZ or F3.CD.IFN-β cells (F3.CD.IFN) at various ratios of astrocytes to F3 cells (1:0, 20:1, and 40:1). (A) Immunofluorescence images of primary astrocytes alone or co-culture (astrocyte:F3 ratio, 40:1) of astrocytes and F3.LacZ, F3.CD.IFN or F3.CD.IFN + 5FC, respectively. Green cells and red cells indicate GFAP-positive astrocytes and DiI-labeled F3 cells, respectively. (B) Subsequently, cells were immunostained with anti-GFAP antibody, and the total numbers of GFAP-positive cells were counted. The number of astrocytes decreased significantly in F3.CD.IFN group. * $P < 0.05$. (C) To evaluate whether TLR-4 is necessary for IFN-β to exert this inhibitory effect on astrocyte growth, DiI-labeled

NSCs were also co-cultured with primary astrocytes derived from TLR-4-deficient mouse in 40:1 ratio. (D) The number of TLR-4-deficient astrocytes did not change.

**Figure 4.** Intravenous administration of F3.CD.IFN-β neural stem cells spares host neural tissue and enhanced axonal regeneration.

(A) Hematoxylin and eosin stained sections of spinal cord injury sites, showing severe destruction of the dorsal half of the spinal cord above the central canal (arrow) and the formation of a granular scar at the injury site.

(B) GFAP immunohistochemical staining, showing hypertrophy of GFAP-positive reactive astrocytes even in the area ventral to the central canal. The intensity of GFAP staining is markedly decreased in the F3.CD.IFN group as compared to that in the other groups.

(C) GFAP density was calculated quantitatively using NIH imaging. * $P < 0.05$.

(D) Neurofilament (NF) immunohistochemical staining. In the PBS and F3.LacZ groups, NF-stained transverse sections demonstrate significant loss of neural fibers. In the F3.CD.IFN + 5FC group, only partial preservation of neural axons is detected. Sections from the F3.CD.IFN group reveal dramatic preservation of fiber number and alignment. (E) Quantification of NF density.*$P < 0.05$.



**Figure 5.** The expression of GFAP and NF at the injury site was compared in mice treated with F3.CD.IFN in the presence or absence of the TLR-4 inhibitor OxPAPC. While the dorsal half of the spinal cord was destroyed equally in every group, the anterior half of the spinal cord was found to be markedly preserved in the F3.CD.IFN group when compared to the F3.CD.IFN+OxPAPC group (A). The intensity of GFAP staining was also significantly decreased in the F3.CD.IFN group as compared to that observed in the F3.CD.IFN+OxPAPC and F3.LacZ groups (B). NF-stained transverse sections also demonstrated a significant loss of neural fibers in the F3.CD.IFN+OxPAPC and F3.LacZ groups, while neural fiber was dramatically preserved in sections from the F3.CD.IFN group (C).

**Figure 6.** Behavioral studies. (A) Basso mouse scale (BMS) for locomotion. We measured the recovery of hindlimb motor function in 7 mice in each treatment group. Animals were evaluated for locomotor recovery at 1, 2, 3, 4, 6, and 8 weeks after the injury. F3.CD.IFN group showed a significant improvement in BMS scores compared to the other 3 groups. Differences between the mean BMS of the F3.CD.IFN group and of the other groups were statistically significant 4 weeks after injury and thereafter (* $P < 0.05$). (B) Inclined plane test. It demonstrates significant recovery of performance 2 weeks following the injury in the F3.CD.IFN group, whereas performance of the other 3 groups remained severely impaired (* $P < 0.05$). (C, D) The improvements in the BMS scores and inclined plane test results that were observed in the F3.CD.IFN group were shown to be inhibited by the OxPAPC TLR-4 inhibitor.



**Figure 7.** Electrophysiology. (A) To measure signal conduction in motor pathways after SCI, transcranial electrical motor nerve evoked-action potentials (MEPs) were measured at 4 and 8 weeks after injury. Animals in the F3.CD.IFN group showed significantly better recovery at both 4 and 8 weeks after injury (* $P < 0.05$). (B) OxPAPC administration in the F3.CD.IFN group significantly worsened the mean MEP amplitude to 178 μV and 228 μV at 4 and 8 weeks, respectively ($p < 0.05$).

**Figure 8.** Assessment of regenerative sprouting of CST axons by 7-T MRI. Four weeks after dorsal hemisection. MRI ( DTI) was performed in mice receiving PBS, F3.LacZ, or F3.CD.IFN. Diffusion tensor of the thoracic spinal cord was visualized. The eigenvectors associated with the tract was depicted as colors according to its orientation; blue illustrates a longitudinal (superior-inferior) orientation. Continuity of this longitudinal tract demonstrated functional regeneration of the axons. In the PBS and F3.LacZ groups, the injury site (arrow) and its surrounding area display high intensity in T2-weighted sagittal sections (arrow

heads), indicating spinal cord edema or necrotic tissue alteration, whereas high intensity is not detected in the F3.CD.IFN group. DTI of the injured spinal cord in the PBS and F3.LacZ groups reveals discontinuity of longitudinal fibers, while these fibers were mostly visible in the F3.CD.IFN group.

A

| Map | Map Folders | Cell process |
|---|---|---|
| Regulation of CDC42 activity | Function groups/G-proteins/RAS-group | small GTPase mediated signal transduction |
| TGF-beta receptor signaling | Cell signaling/Growth and differentiation/Growth and differentiation (common pathways) Function groups/Growth factors | intracellular receptor-mediated signaling pathway, response to extracellular stimulus |
| Cell-matrix glycoconjugates | Cell signaling/Cell adhesion | cell adhesion |
| The metaphase checkpoint | Cell signaling/Cell cycle control | cell cycle |
| IL1 signaling pathway | Cell signaling/Immune response Function groups/Cyto/chemokines | cytokine and chemokine mediated signaling pathway, immune response |
| Transcription regulation of granulocyte development | Cell signaling/Growth and differentiation/Hematopoiesis | response to extracellular stimulus |
| Toll-like receptor (TLR) ligands and common TLR signaling pathway leading to cell proinflammatory response | Cell signaling/Immune response | immune response |

B

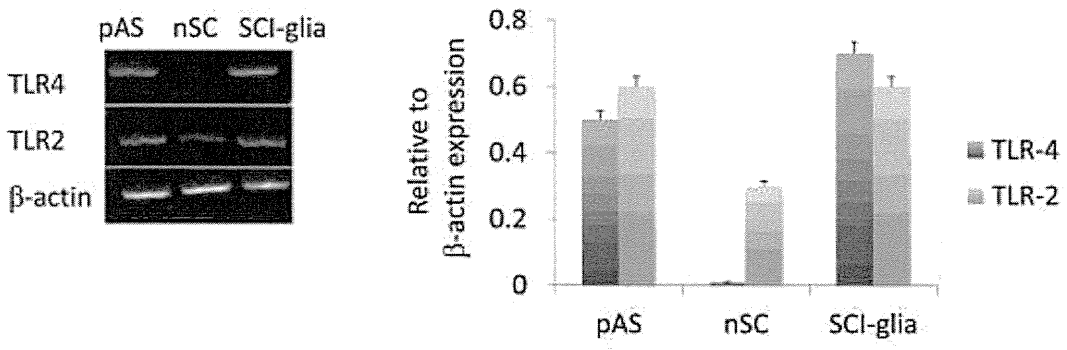


Figure 1

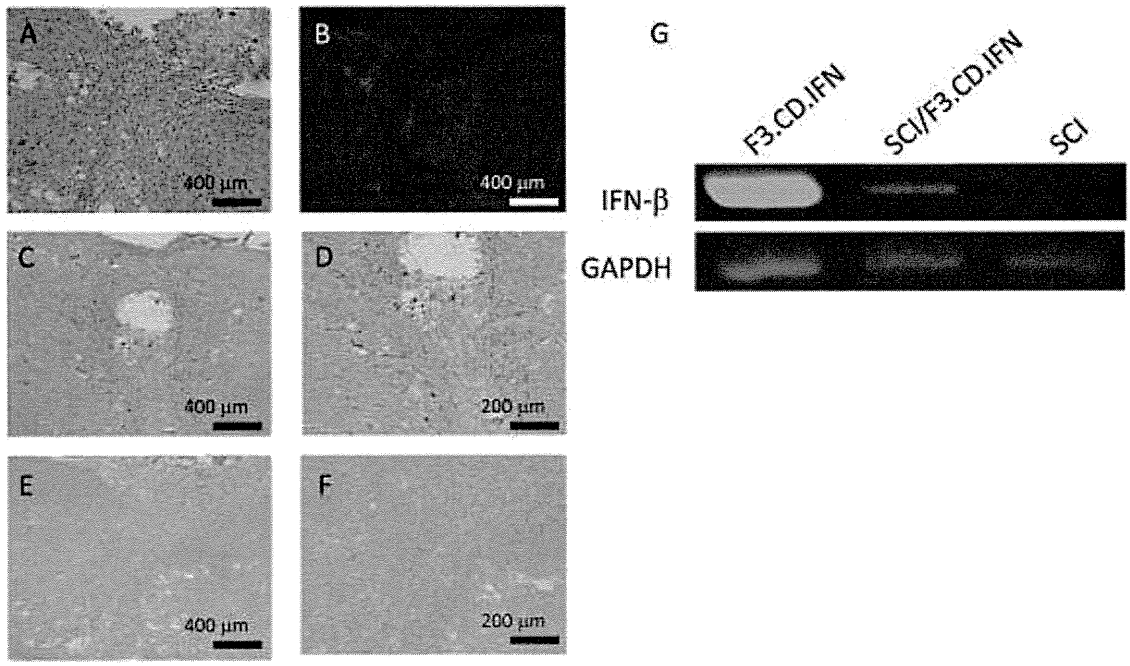


Figure 2

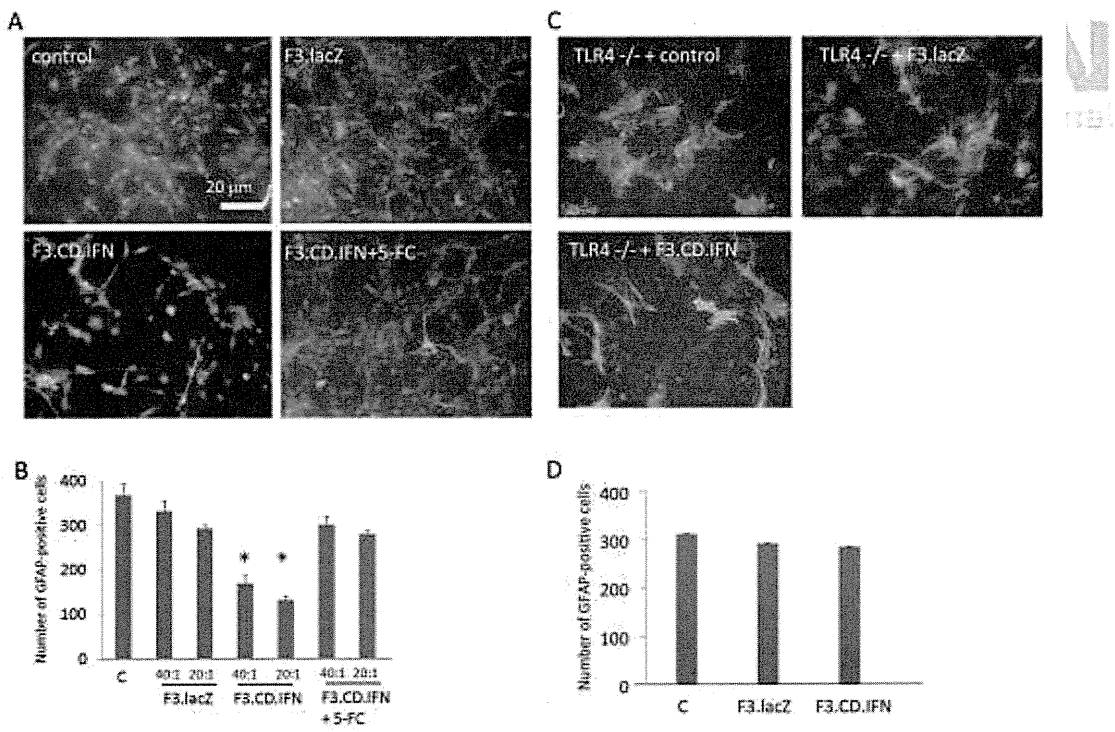


Figure 3

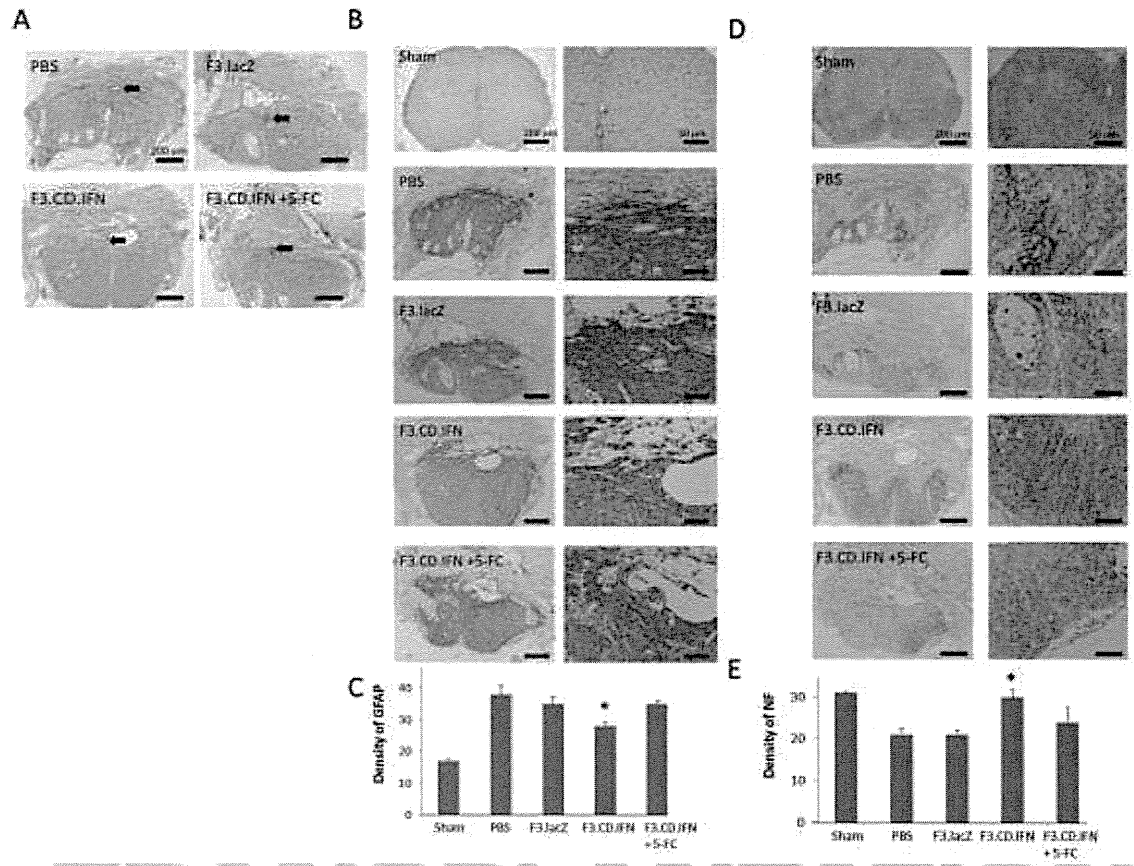


Figure 4

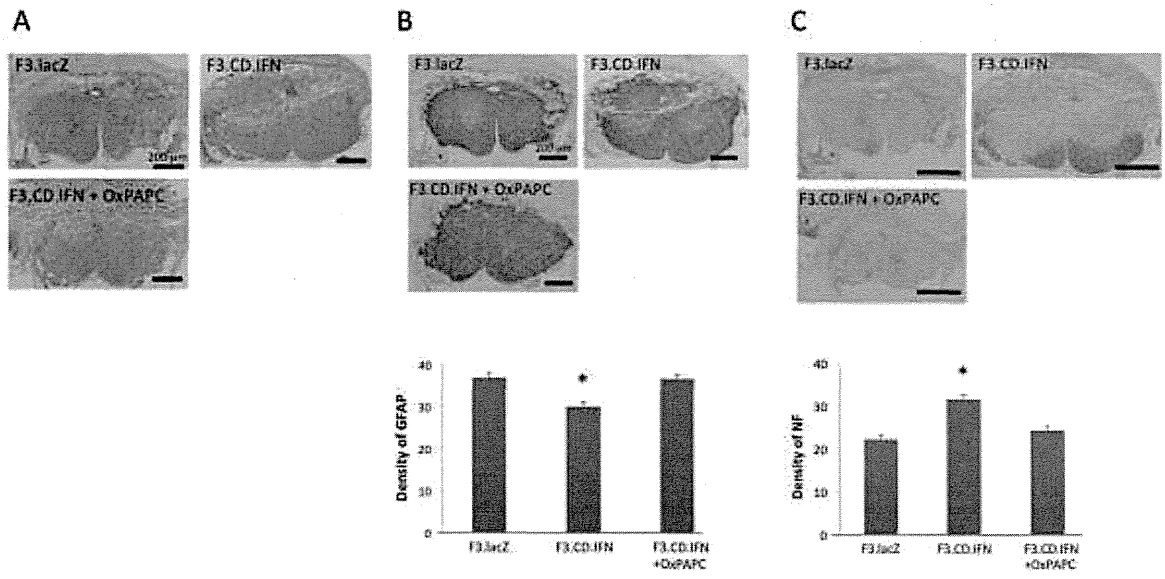


Figure 5

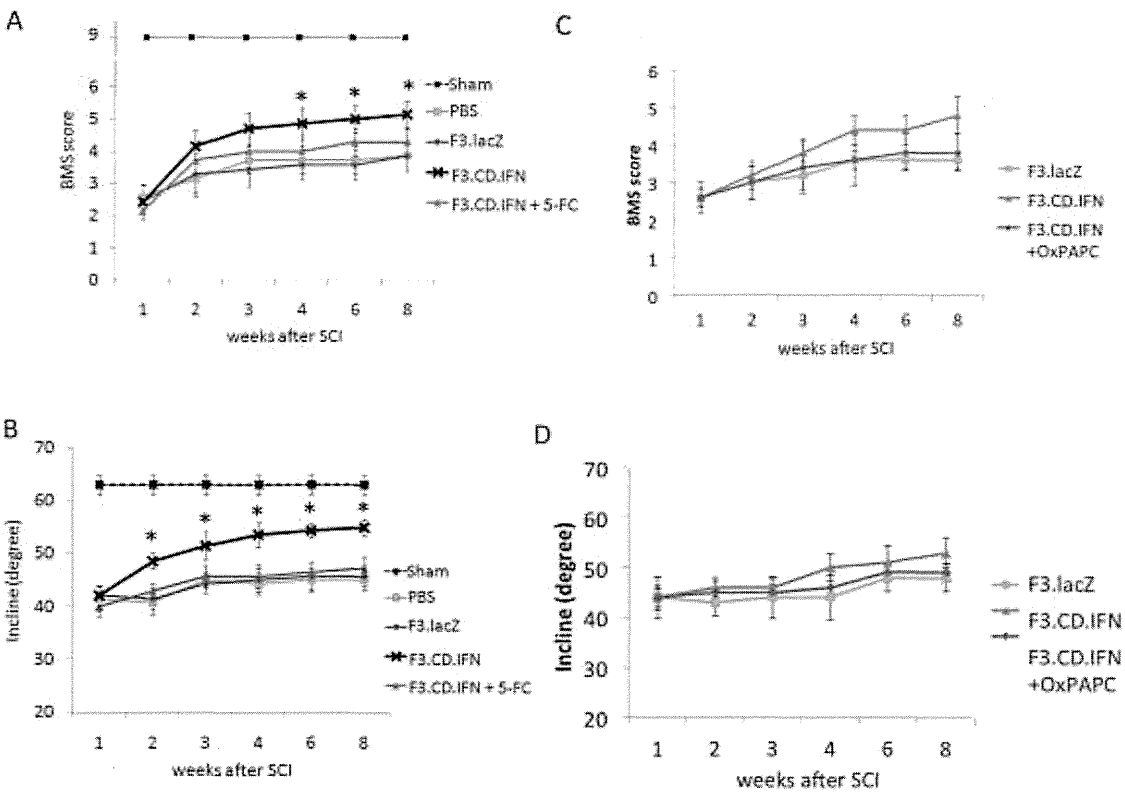


Figure 6

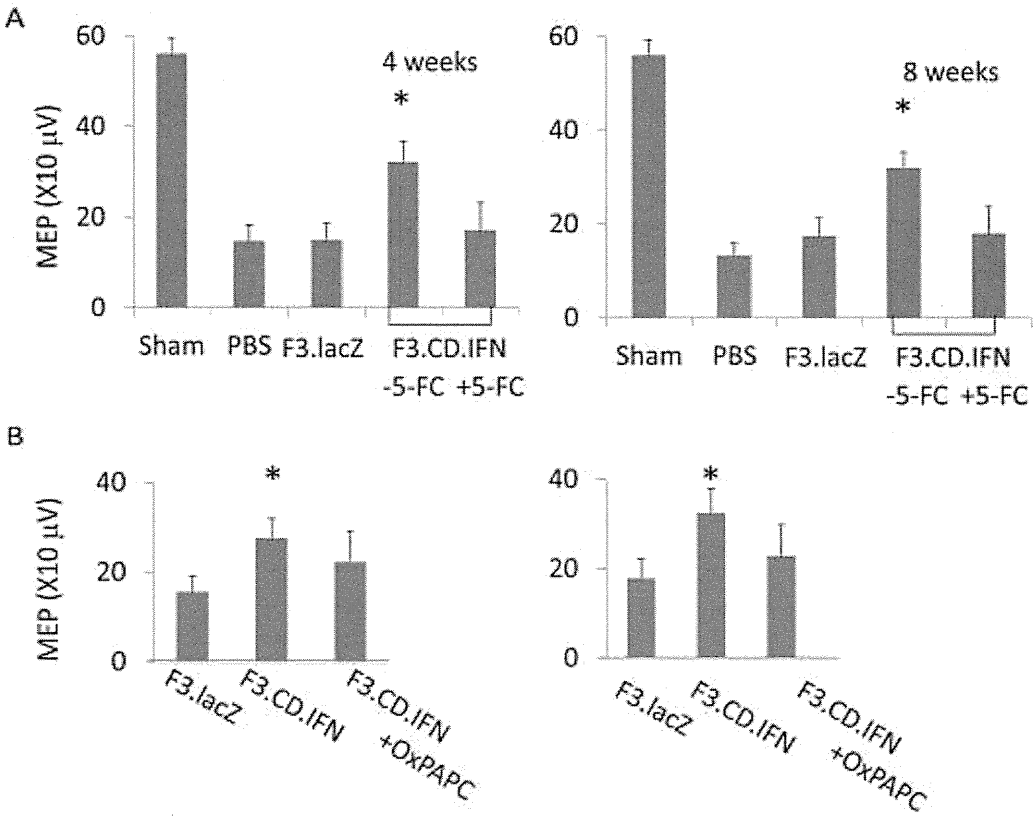




Figure 7

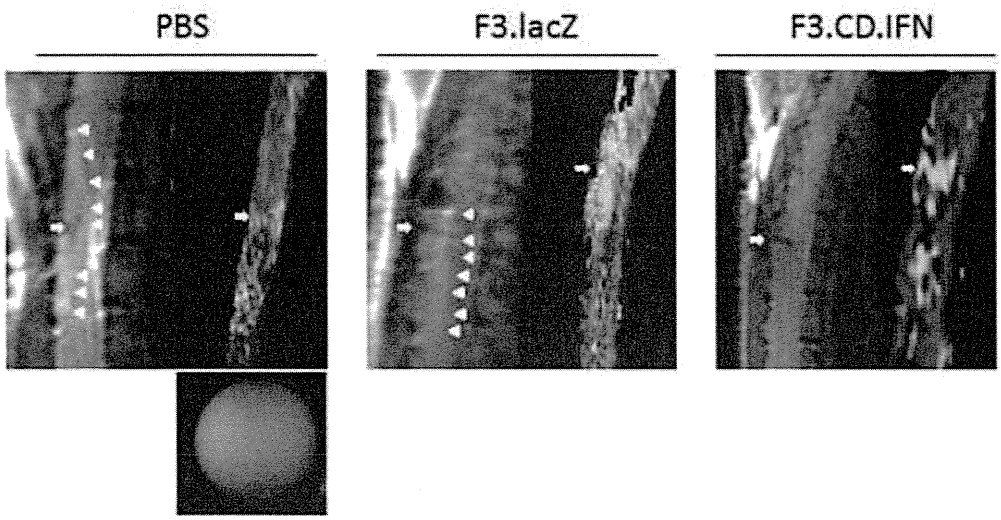


Figure 8

Published OnlineFirst March 26, 2013; DOI: 10.1158/1078-0432.CCR-12-3726

Clinical Cancer Research

# Tissue Redox Activity as a Hallmark of Carcinogenesis: From Early to Terminal Stages of Cancer

Rumiana Bakalova, Zhivko Zhelev, Ichio Aoki, et al.

*Clin Cancer Res* 2013;19:2503-2517. Published OnlineFirst March 26, 2013.

Published OnlineFirst March 26, 2013; DOI: 10.1158/1078-0432.CCR-12-3726

Clinical Cancer Research

*Imaging, Diagnosis, Prognosis*

# Tissue Redox Activity as a Hallmark of Carcinogenesis: From Early to Terminal Stages of Cancer

Rumiana Bakalova[1,2], Zhivko Zhelev[1,3], Ichio Aoki[1], and Tsuneo Saga[1]

## Abstract

**Purpose:** The study aimed to clarify the dynamics of tissue redox activity (TRA) in cancer progression and assess the importance of this parameter for therapeutic strategies.

**Experimental Design:** The experiments were carried out on brain tissues of neuroblastoma-bearing, glioma-bearing, and healthy mice. TRA was visualized *in vivo* by nitroxide-enhanced MRI on anesthetized animals or *in vitro* by electron paramagnetic resonance spectroscopy on isolated tissue specimens. Two biochemical parameters were analyzed in parallel: tissue total antioxidant capacity (TTAC) and plasma levels of matrix metalloproteinases (MMP).

**Results:** In the early stage of cancer, the brain tissues were characterized by a shorter-lived MRI signal than that from healthy brains (indicating a higher reducing activity for the nitroxide radical), which was accompanied by an enhancement of TTAC and MMP9 plasma levels. In the terminal stage of cancer, tissues in both hemispheres were characterized by a longer-lived MRI signal than in healthy brains (indicating a high-oxidative activity) that was accompanied by a decrease in TTAC and an increase in the MMP2/MMP9 plasma levels. Cancer progression also affected the redox potential of tissues distant from the primary tumor locus (liver and lung). Their oxidative status increased in both stages of cancer.

**Conclusions:** The study shows that tissue redox balance is very sensitive to the progression of cancer and can be used as a diagnostic marker of carcinogenesis. The study also suggests that the noncancerous tissues of a cancer-bearing organism are susceptible to oxidative damage and should be considered a therapeutic target. *Clin Cancer Res; 19(9); 2503–17. ©2013 AACR.*

## Introduction

Redox signaling plays a crucial role in carcinogenesis (1–4). The increase in cellular oxidants [e.g., reactive oxygen species (ROS) and reactive nitrogen species (RNS)] above a critical level triggers genomic instability and uncontrolled proliferation (1–7), which causes normal cells to become malignant.

Cancer cells are also characterized by an abnormal production of reducing equivalents as a result of accelerated glycolysis (Warburg effect) and the pentose phosphate cycle and by a rapid consumption of these reducers to maintain accelerated anabolism, which is necessary for cell proliferation and immortalization (1, 2, 7, 8). Cancer cells also require high amounts of antioxidants to maintain an ROS/RNS level that is below the threshold for the induction of apoptosis and cell death, but is sufficiently high to ensure genomic instability (1, 7, 9, 10). All of these processes provoke redox imbalance in cancer, which is a hallmark of carcinogenesis. The tissue redox status could be a diagnostic marker, a therapeutic target, and a marker for the evaluation and planning of a therapeutic strategy in real time.

The primary endogenous triggers of redox imbalance in cancer are defective mitochondria and NADPH oxidase complexes. These triggers are involved simultaneously in 2 processes that affect tissue redox status: (i) an excessive generation of ROS (in particular, superoxide and/or hydrogen peroxide) and RNS and (ii) an increased consumption of 3 of the major cellular reducers, as NADH, NADPH, and glutathione (1, 11–18). The high-oxidative activity of cancerous tissue is known despite the hypoxia that occurs in solid tumors. The oxidative capacity of cancer cells is due to abnormal ROS/RNS levels and is not necessarily associated with a high oxygen tension. It is widely accepted that cancer cells are characterized by increased ROS/RNS production compared with that of normal cells that ensure genomic instability (1–15). ROS and RNS are involved in hypoxic signaling pathways and have important implications for the adaptation of cancer to oxidative stress, the induction of uncontrolled proliferation, and immortalization.

Most likely, there is a significant difference between the redox activity of the tumor core and periphery in addition to

**Authors' Affiliations:** [1]Diagnostic Imaging Program, Molecular Imaging Center, National Institute of Radiological Sciences, Inage-ku, Chiba, Japan, [2]Medical Faculty, Sofia University "St. Kliment Ohridski", Sofia; and [3]Medical Faculty, Trakia University, Stara Zagora, Bulgaria

**Corresponding Author:** Rumiana Bakalova, National Institute of Radiological Sciences, 4-9-1 Anagawa, Inage, Chiba 263-8555, Japan. Phone: 81-43-206-4067; Fax: 81-43-206-4067; E-mail: bakalova@nirs.go.jp

**doi:** 10.1158/1078-0432.CCR-12-3726

Published OnlineFirst March 26, 2013; DOI: 10.1158/1078-0432.CCR-12-3726



## Translational Relevance

This study directly relates to cancer diagnosis, the assessment of cancer progression (from early to terminal stage), and planning a therapeutic strategy. This study shows that tissue redox balance is very sensitive to cancer development and can be used as a diagnostic marker of carcinogenesis. The method is simple and applicable on isolated tissue and blood specimens. The method shows the potential for promising application in molecular imaging diagnostic *in vivo* on humans following the development of cell-penetrating nitroxide probes with high contrast, low toxicity, and minimal side effects.

The most important observations are that the oxidative status of noncancerous tissues (even those distant from the primary tumor locus) increases with cancer progression and that these tissues become susceptible to oxidative stress and damage.

tumors in different stages (i.e., early, intermediate, and terminal) of development. However, there are methodologic restrictions that hamper the visualization and evaluation of such a difference *in vivo*. There is no suitable sensor platform for real-time imaging of tissue redox activity (TRA) that is characterized by high sensitivity and resolution.

Recently, we reported a noninvasive methodology for the estimation of TRA on intact mammals, allowing a differentiation of cancer development from normal (healthy) conditions (19–21). The method is based on the redox cycle of cell-penetrating nitroxide derivatives and their MRI and electron paramagnetic resonance (EPR) contrast properties, which make them useful molecular sensors for TRA (Fig. 1).

*In vitro* studies indicate that the contrast-enhancing nitroxide radical could be converted rapidly to the noncontrast-enhancing hydroxylamine and/or oxoammonium by different cellular compounds (e.g., free ions of transition metals, hydroxyl and hydroperoxyl radicals, ubiquinols, NAD(P)H, and ascorbate/dehydroascorbate; Fig. 1; refs. 22–28). In turn, hydroxylamine and oxoammonium are "superoxide dismutase mimetics" and could restore the nitroxide radical (22, 26, 29). The logarithmic acid dissociation constant value of 4.8 is reported for the equilibrium between superoxide anion and its protonated form, that is, the hydroperoxyl radical. The interaction of oxoammonium with superoxide occurs at pH < 4.5, whereas under physiologic conditions (pH ~ 7.4) the oxoammonium is reduced to hydroxylamine by NAD(P)H (26). The interaction of hydroxylamine with superoxide occurs at approximately pH 7.4 with the release of hydrogen peroxide and restoration of the radical form of the nitroxide (26). Ui and colleagues have reported that the exposure to hydrogen peroxide inhibits the reduction of the nitroxide radical *in vivo*, and hydrogen peroxide reoxidizes hydroxylamine to the original radical form (22, 30). It seems that *in vivo*, nitroxide exists primarily in 2 forms: as a radical and as hydroxylamine. Various reducers and oxidizers are involved (directly or indirectly) in the formation of hydroxylamine, but only the interaction of hydroxylamine with superoxide and/or hydrogen peroxide seems to dominate *in vivo* as the process that restores the nitroxide radical and its MRI/EPR contrast.

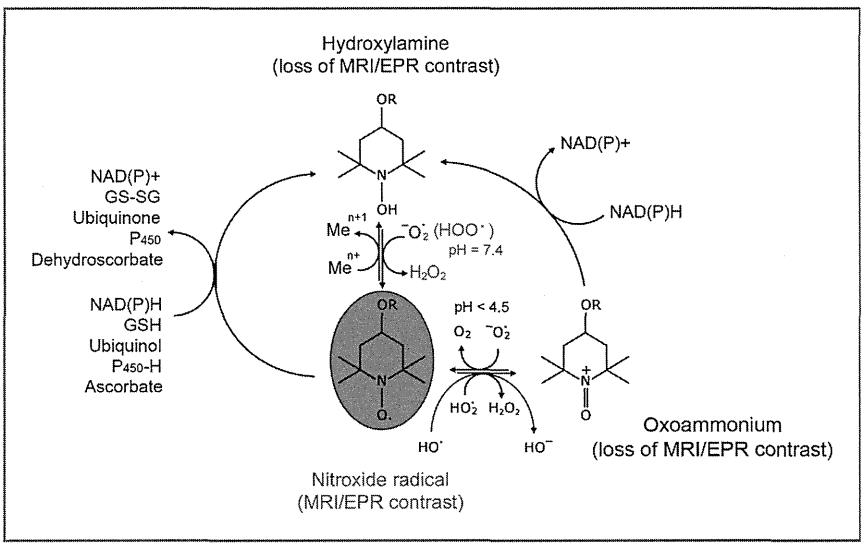


Figure 1. Nitroxide redox cycle as a sensing platform for the imaging of TRA: principle of the method. *In vitro* studies show that the nitroxide radical, which is characterized by MRI/EPR contrast enhancement, can be converted to the noncontrast hydroxylamine and/or oxoammonium by different compounds in cells and body fluids (e.g., free ions of transition metals, hydroxyl and hydroperoxyl radicals, ubiquinols, NAD(P)H, ascorbate, glutathione, etc.). The contrast-enhancing radical form can be recovered by interaction of hydroxylamine with the superoxide radical at physiologic, pH (7.4), or interaction of oxoammonium with the superoxide radical at pH < 4.5. Thus, the nitroxide-enhanced MRI/EPR signal follows the reduction/oxidation of the nitroxide derivative and indicates the redox status of tissues and body fluids.

Published OnlineFirst March 26, 2013; DOI: 10.1158/1078-0432.CCR-12-3726



Briefly, the nitroxide radical participates in electron transfer reactions with oxidizers and reducers with the formation of contrast-enhancing or noncontrast intermediate products (31–33). The rate constants of these reactions determine the intensity of the nitroxide-enhanced MRI/EPR signal in living cells and tissues. In healthy mammals, the intensity, duration, and/or half-life of the nitroxide-enhanced MRI/EPR signal ($\tau_{1/2}$) in the selected region of interest (ROI; e.g., cells, tissues, bloodstream) can be considered a reference value for the redox activity of the respective specimen in normal conditions (healthy organism; ref. 19). Any significant deviation from this reference value indicates a redox imbalance, such as the high-oxidative or reducing activity of cells, tissues, or physiologic fluids. In previous studies, we established that in cancer-bearing mammalian tissues, the intensity, duration, and $\tau_{1/2}$ values were completely different from the respective reference values and that this parameter is a valuable diagnostic marker for carcinogenesis (19–21).

The EPR contrast of the nitroxide radical allows the determination of the exact concentration and redox status of the nitroxide derivative in the respective tissue and/or cells using EPR spectroscopy or imaging (EPRI; refs. 31–35). The comparative analysis of the results, obtained using both imaging techniques, gives accurate information about the TRA *in vivo*.

The reduction/oxidation of nitroxide is spatially separated and occurs in (i) the bloodstream, (ii) the extracellular–extravascular space (EES) of the tissue, and (iii) the cells of the tissue. The MRI/EPR signal dynamics is a result of various factors and processes that occur simultaneously in the following 4 areas: (i) the lifetime of the nitroxide in the circulation, depending on its water solubility (35, 36), (ii) the reduction/oxidation of the nitroxide in the bloodstream, which is expected to be low in the plasma but sufficiently high in blood cells (if it penetrates cell membranes; refs. 35, 36), (iii) the penetration and accumulation of the nitroxide in the EES and its reduction/oxidation, which is expected to be negligible, and (iv) the penetration and accumulation of the nitroxide in the cells of the tissue and its intracellular reduction/oxidation, which is expected to be substantial in comparison with the bloodstream and EES (20, 37). TRA is a combination of the redox capacity of the extracellular (EES) and intracellular space of the tissue. The metabolism and/or clearance of nitroxide from the organism is not related to the redox activity of the tissues and physiologic fluids and should be negligible during short-term scanning.

The hydrophilic nitroxides are characterized by a long lifetime in the circulation and a very slow penetration or no penetration into the cells. In contrast, the hydrophobic (and amphiphilic) nitroxides are characterized by a short lifetime in the circulation and an easy penetration into the EES and cells. Therefore, only the hydrophobic cell-penetrating nitroxides are appropriate molecular sensors for MRI/EPRI of TRA, especially *in vivo*.

This study aims to clarify the difference between TRAs in different stages of cancer development *in vivo*. For this purpose, we used 2 cancer models (neuroblastoma- and glioma-bearing mice), blood–brain barrier (BBB)-penetrating and cell-penetrating nitroxide derivatives, and nitroxide-enhanced MRI and EPR spectroscopy.

## Materials and Methods

### Chemicals

2,2,6,6-tetramethylpiperidine-1-oxyl–labeled nitrosourea (SLENU) was synthesized according to the procedure described by Gadjeva (38). SLENU is a spin-labeled analog of the conventional anticancer drug 1-(2-chloroethyl)-3-cyclohexyl-1-nitrosourea (Lomustine). 4-hydroxy-2,2,6,6-tetramethylpiperidine 1-oxyl (TEMPOL) was purchased from Sigma-Aldrich (cat. No. 176141).

### Cancer models and experimental design

All experiments were carried out in accordance with the guidelines of the Physiological Society of Japan and were approved by the Animal Care and Use Committee of the National Institute of Radiological Sciences (NIRS; Chiba, Japan).

The mice (nude *Balb/c*; male) were separated into the following groups: healthy mice (controls) and cancer-bearing mice with brain neuroblastoma or glioma. In all groups, the mice were of identical age, nearly identical weight (23 ± 3 g), and maintained under identical conditions.

Two cancer models were developed using *Neuro2a* (neuroblastoma) or *U87* (glioma) cells. Cancer cells ($0.5 \times 10^5$ cells in 10 μL) were grafted in one hemisphere of the brain. Anatomically visualized brain neuroblastoma or glioma developed within approximately 9 or 20 days after inoculation, respectively.

The mice were subjected to MRI measurements on the third and ninth day after the inoculation of *Neuro2a* cells or on the seventh and 20th day after inoculation of *U87* cells, when the cancer was in the early and intermediate/terminal stage of its development, respectively.

In preliminary experiments, we investigated the effect of "sham tumor inoculation" (using 10 μL of PBS) on the dynamics of the nitroxide-enhanced MRI signal. Because there was no difference between inoculated and noninoculated hemispheres, or between untreated healthy mice and mice with "sham tumor inoculation," we used untreated healthy mice as controls in this study.

### *In vivo* MRI measurements

MRI measurements were conducted on a 7.0 Tesla horizontal magnet (Kobelco and Jastec) interfaced to a Bruker Avance console (Bruker BioSpin) and controlled with the ParaVision 4.0.1 program (Bruker BioSpin).

The mice were anesthetized by isoflurane (1.2%) and placed in a head or body holder (RAPID Biomedical). A respiration sensor (SA Instruments Inc.) was placed on the back of the mice. A temperature probe (FOT-M and FTI-10, FISO Technologies Inc.) was used to monitor the rectal temperature. The tail vein was cannulated using a polyethylene tube (PE-10, Becton-Dickinson) for the drug injection. The mouse was placed in the $^1$H-volume

Published OnlineFirst March 26, 2013; DOI: 10.1158/1078-0432.CCR-12-3726



radio-frequency resonator (Bruker BioSpin) with surface radio-frequency receiver (RAPID Biomedical), which was prewarmed using a body temperature controller (RAPID Biomedical). The resonator units, including the mouse, were placed in the magnet bore. The body temperature was maintained at 37 ± 1°C during the MRI measurements.

Five control images of the mouse brain or body were taken before injection with the following parameters: $T_1$ -weighted incoherent gradient-echo sequence (fast low-angle shot), repetition time = 75 ms; echo time = 3.5 ms; flip angle = 45°; field of view = 3.2 × 3.2 cm; number of averages = 4; scan time = 19.6 seconds; matrix = 64 × 64; slice thickness = 1.0 mm; and number of slices = 4. A solution of nitroxide derivative [SLENU, dissolved in dimethyl sulfoxide (DMSO), or TEMPOL, dissolved in 10 mmol/L PBS, pH 7.4, and reduced by ascorbate, 1:1, mol: mol; 100 mmol/L stock solutions] was injected via the tail vein (100 μL/25 g mouse; 0.4 μmol/g body weight) 1 minute and 40 seconds after beginning the scan. $T_1$-weighted images were acquired continuously within approximately 14 minutes, using the parameters described above. Mice injected with DMSO served as negative controls. DMSO did not act as a radical scavenger under the experimental conditions described above. TEMPOL, dissolved in DMSO, produced an identical nitroxide-enhanced MRI signal (as intensity and profile) in anesthetized mice as TEMPOL dissolved in PBS. The final dose of each nitroxide was lower than the $LD_{50}$ value calculated for intravenous administration in wild-type mice (38).

The MRI data were analyzed using ImageJ software (NIH, Bethesda, MD). The averaged value of the first 5 control sequences (recorded before injection) was calculated, and each sequence of the kinetic measurement was normalized to this averaged value by division using an identical algorithm to that presented by Zhelev and colleagues (39).

### *In vitro* EPR measurements

The mice were euthanized, and the brain, lung, and liver were isolated. The tissues were homogenized in a 4-fold volume of PBS. Protein concentration was measured using the Bradford method, and each homogenate was diluted to 10 mg protein/mL. Noncontrast-enhancing reduced TEMPOL (dissolved in 10 mmol/L PBS, pH 7.4, and reduced by ascorbate; 1:1, mol:mol) was added to the tissue homogenate (final concentration of TEMPOL: 10 mmol/L). The sample (100 μL) was placed into a glass capillary, and X-band EPR spectra were recorded on an X-band EPR instrument (Bruker) with a transverse electric–mode cavity. The measurements were conducted under the following conditions: microwave frequency = 9.4 GHz; magnetic field strength = 336 mT; microwave power = 2.0 mW; field modulation frequency = 100 kHz; field modulation amplitude = 0.063 mT; time constant = 0.01 seconds; sweep width = 10 mT; and scan time (sweep time) = 1 minute (39). The EPR spectra were recorded before and after the addition of reduced TEMPOL. The data were normalized to 1 mg protein/mL.

### *In vitro* total antioxidant capacity assay

The total antioxidant capacity (TAC) in isolated tissue homogenates was analyzed using the OxiSelect Total Antioxidant Capacity Assay Kit (Cell Biolabs Inc.), according to the manufacturer's instructions. The samples were analyzed photometrically at 490 nm using the microplate reader "Tecan Infinite F200 PRO" (Tecan Austria GmbH).

### Analysis of plasma MMP2 and MMP9 levels

The plasma samples were obtained from healthy and neuroblastoma-bearing mice. ELISA was used to determine plasma total matrix metalloproteinases (MMP)2 and total MMP9 levels, according to the manufacturer's instructions. The MMP2 ELISA Kit [Human/Mouse/Rat MMP2 (total), Quantikine; R&D Systems Inc.] detects pro-, active, and tissue inhibitor of metalloproteinase (TIMP)-complexed MMP2. The MMP9 ELISA Kit [Mouse MMP9 (total), Quantikine; R&D Systems Inc.] detects pro-, active, and TIMP-complexed MMP9.

### Statistical analysis

The data were statistically analyzed by ANOVA using Student *t* test.

## Results

### Early stage of brain neuroblastoma

Figure 2 shows typical images of the extracted nitroxide-enhanced MRI signal (normalized to the baseline) in healthy (Fig. 2A) and neuroblastoma-bearing mice in the early stage of cancer (3 days after inoculation of cancer cells into the brain; Fig. 2B). In this stage, the tumor cannot be detected anatomically even with high- resolution MRI (spin-echo sequence). The images from both experimental groups were similar. The averaged kinetic curves, however, showed that there was a significant difference in the duration and half-life ($\tau_{1/2}$) of the nitroxide-enhanced MRI signal between control and neuroblastoma-bearing mice (Fig. 2C and D).

Two ROIs were selected: (i) the brain area (ROI1) and (ii) the surrounding (nonbrain) area (ROI2; Fig. 2A, a). In both ROIs, the signal increased after the injection of nitroxide followed by a rapid or slower decrease to the baseline. The enhancement of the MRI signal in the beginning is due to the presence of nitroxide in the blood and its penetration and accumulation in the subsequent tissue, whereas the decrease is due to its reduction to noncontrast hydroxylamine, which occurs predominantly in cells.

In the brain area (ROI1) of healthy mice, the half-life of the nitroxide-enhanced MRI signal ($\tau_{1/2}$) was approximately 80 seconds and the duration of the signal was approximately 5 minutes and 40 seconds, and these values can be considered a reference for the TRA of the normal brain (Fig. 2C, gray curve). The profile of the histograms indicates a high reducing activity of normal brain tissue for the nitroxide radical. In ROI1 of neuroblastoma-bearing mice, $\tau_{1/2}$ was approximately 56 seconds and the duration of the signal was approximately 3 minutes, which is significantly

Published OnlineFirst March 26, 2013; DOI: 10.1158/1078-0432.CCR-12-3726



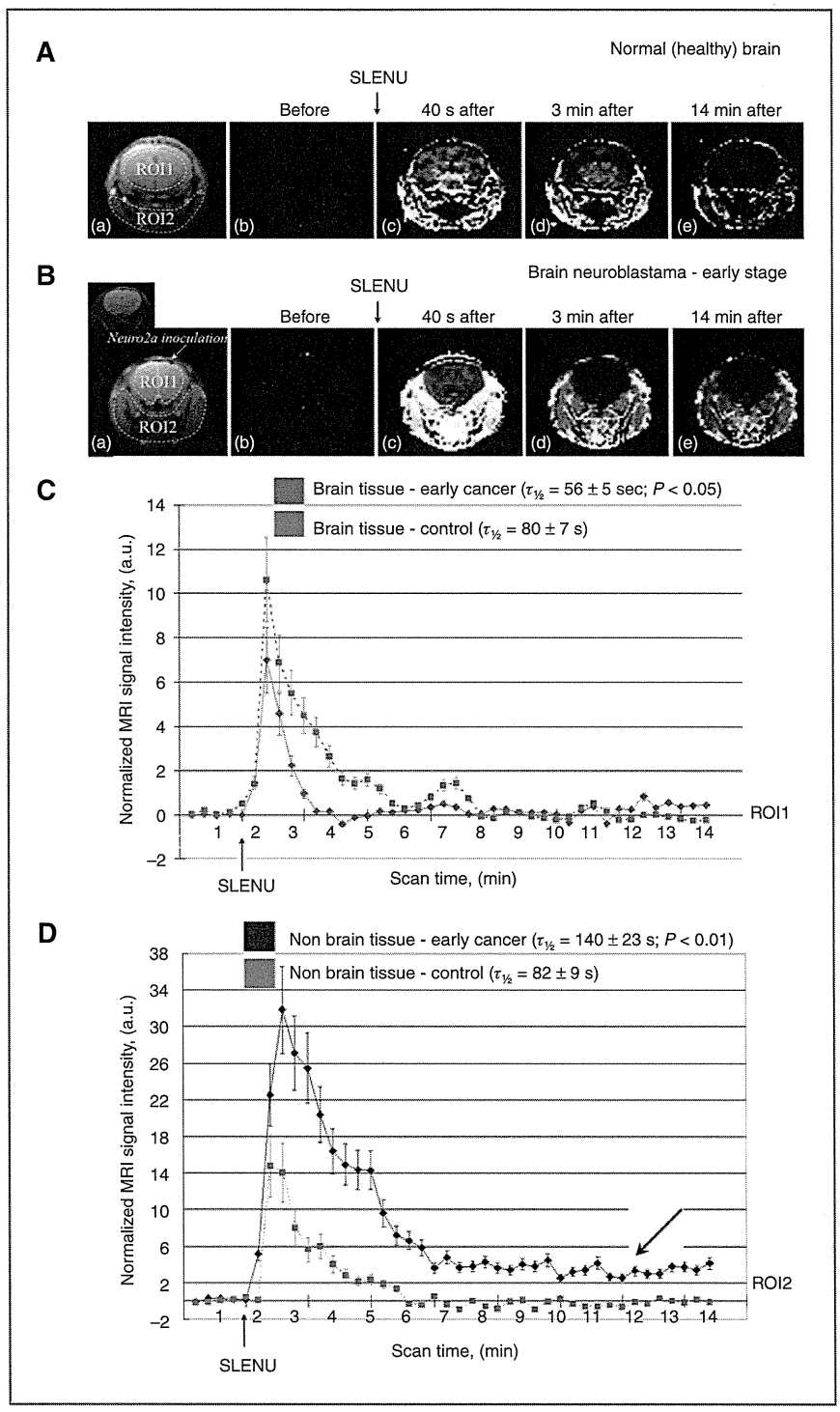


Figure 2. Healthy and neuroblastoma-bearing mice (early stage of cancer development). A and B, typical MR images of healthy brain (A) and neuroblastoma-bearing brain in the early stage of cancer (B): a, MR image of mouse brain; b, extracted nitroxide-enhanced MRI signal obtained before (baseline; b); and after injection of nitroxide (SLENU; c, d, e). C and D, kinetics of the nitroxide-enhanced MRI signal in the brain (ROI1; C) and surrounding (nonbrain) tissues (ROI2; D) obtained before and after injection of SLENU. Control kinetics (gray dotted lines) obtained in healthy mice are given for comparison. The data are the mean ± SD from 10 animals for the control group and 7 animals for the neuroblastoma-bearing group. ROIs are indicated by dotted lines on MR images. SLENU was in the oxidized (radical) form.

Published OnlineFirst March 26, 2013; DOI: 10.1158/1078-0432.CCR-12-3726



shorter than that of control mice ($P < 0.05$; Fig. 2C, red curve). This result indicates that the reducing capacity of the brain tissue in the early stage of brain neuroblastoma was higher than that of the control brain.

In the surrounding (nonbrain) tissues (ROI2), the opposite tendency was observed (Fig. 2D). In healthy mice, the half-life of the MRI signal was significantly shorter than that in the neuroblastoma-bearing mice; approximately 82 seconds versus approximately 140 seconds, respectively ($P < 0.01$). The duration of the signal in neuroblastoma-bearing mice was more than 14 minutes versus 5 minutes and 40 seconds in healthy mice. This result indicates that the reducing activity of nonbrain tissues in the early stage of neuroblastoma is lower than that in the control group. In neuroblastoma-bearing mice, the MRI signal did not reach the baseline within 14 minutes of continuous scanning (Fig. 2D, blue curve), which indicates that the oxidation of nitroxide dominates over reduction.

**Terminal stage of brain neuroblastoma**

In the terminal stage of brain neuroblastoma (9 days after inoculation), the kinetics of the nitroxide-enhanced MRI signal in the brain and nonbrain tissues were completely different from the reference profiles, recorded for the control group, and from the profiles of the early neuroblastoma group (Fig. 3B and C). Three ROIs were selected: (i) the cancerous hemisphere (ROI1), (ii) the noncancerous hemisphere (ROI2), and (iii) the surrounding (nonbrain) area (ROI3; Fig. 3A, a). The cancer was visualized anatomically by MRI.

In ROI1 and ROI2, the signal increased after injection and reached a plateau without a decrease within 14 minutes ($\tau_{1/2} > 14$ minutes; $P < 0.001$ vs. control). In ROI3, the signal increased after injection then decreased slowly without reaching the baseline within 14 minutes ($\tau_{1/2} \sim 14$ minutes; $P < 0.001$ vs. control). The histograms indicate a high-oxidative activity of the cancerous and noncancerous tissues of neuroblastoma-bearing mice for the nitroxide. In all ROIs of neuroblastoma-bearing mice, the duration of the signal was more than 14 minutes versus 5 minutes and 40 seconds in controls.

The kinetics of the MRI signal showed identical profiles in both hemispheres of the neuroblastoma-bearing brain (Fig. 3B); however, the signal intensity was significantly higher in the cancerous area than in the noncancerous hemisphere (Figs. 2B and 3A).

**Early stage of brain glioma**

Figure 4A shows a typical image of brain glioma in the early stage of development (9 days after the inoculation of cancer cells into the brain). The tumor is very small but can be visualized anatomically using high-resolution MRI (spin-echo sequence). Two ROIs were selected: (i) the brain area (ROI1) and (ii) the surrounding (nonbrain) area (ROI2; Fig. 4A).

In ROI1 of glioma-bearing mice, the half-life of the MRI signal decay was significantly shorter than that in control mice (~63 seconds vs. 80 seconds, respectively; $P < 0.05$); the duration of the signal was approximately 3 minutes versus approximately 5 minutes and 30 seconds in controls (Fig. 4B, red curve). This result indicates that the reducing activity of the brain tissue in the early stage of brain glioma is higher than that of the control brain.

In the surrounding tissues (ROI2), an opposite tendency was observed (Fig. 4C). In healthy mice, the half-life of the MRI signal was significantly shorter than that in the glioma-bearing mice; approximately 82 seconds versus approximately 180 seconds, respectively ($P < 0.01$). The duration of the signal in glioma-bearing mice was more than 14 minutes versus approximately 5 minutes and 40 seconds in control mice. This result indicates that the reducing activity of nonbrain tissues in the early stage of brain glioma is lower than that in the control group. In glioma-bearing mice, the MRI signal did not reach the baseline within 14 minutes of continuous scanning (Fig. 4C, blue curve), which indicates that the oxidation of nitroxide dominates over reduction.

**Terminal stage of brain glioma**

In the terminal stage of brain glioma (20 days after inoculation), the kinetics of the nitroxide-enhanced MRI signal in the brain and nonbrain tissues were completely different from the reference profiles that were recorded for the control group (Fig. 5B and C). Three ROIs were selected: (i) the cancerous hemisphere (ROI1), (ii) the noncancerous hemisphere (ROI2), and (iii) the surrounding (nonbrain) area (ROI3; Fig. 5A, a). The cancer was visualized anatomically by MRI.

In ROI2, the signal increased after injection and reached a plateau without a decrease within 14 minutes ($\tau_{1/2} > 14$ minutes; $P < 0.001$ vs. control). In ROI1 and ROI3, the signal increased after injection then decreased slowly without reaching the baseline within 14 minutes (in ROI3: $\tau_{1/2} \sim 440$ seconds; $P < 0.001$ vs. control; in ROI2: $\tau_{1/2} \sim 330$ seconds; $P < 0.001$ vs. control). The histograms indicate a high-oxidative activity of the cancerous and noncancerous tissues of glioma-bearing mice for the nitroxide.

The kinetics of the MRI signal showed identical profiles in both hemispheres of the glioma-bearing brain. However, the signal intensity was significantly higher in the cancerous area than in the noncancerous hemisphere (Fig. 5A, b).

**Tissue-oxidizing capacity *in vivo* and *in vitro***

To verify the data from the nitroxide-enhanced MRI *in vivo*, we used a second experimental strategy. Nitroxide (TEMPOL) was reduced until there was a complete loss of the MRI and EPR contrast. The reduced noncontrast-enhancing form was injected in anesthetized mice (healthy and cancer bearing), and the dynamics of the nitroxide-enhanced MRI signal were detected under identical conditions, as in Figs. 2 and 3.

The data in Fig. 6A indicate that the nitroxide-enhanced MRI signal appeared and increased within 14 minutes of continuous scanning only in the brain of neuroblastoma-bearing mice in the terminal stage of cancer (red and yellow curves). The signal intensity was higher in the cancerous hemisphere than in the noncancerous hemisphere. In the

Published OnlineFirst March 26, 2013; DOI: 10.1158/1078-0432.CCR-12-3726



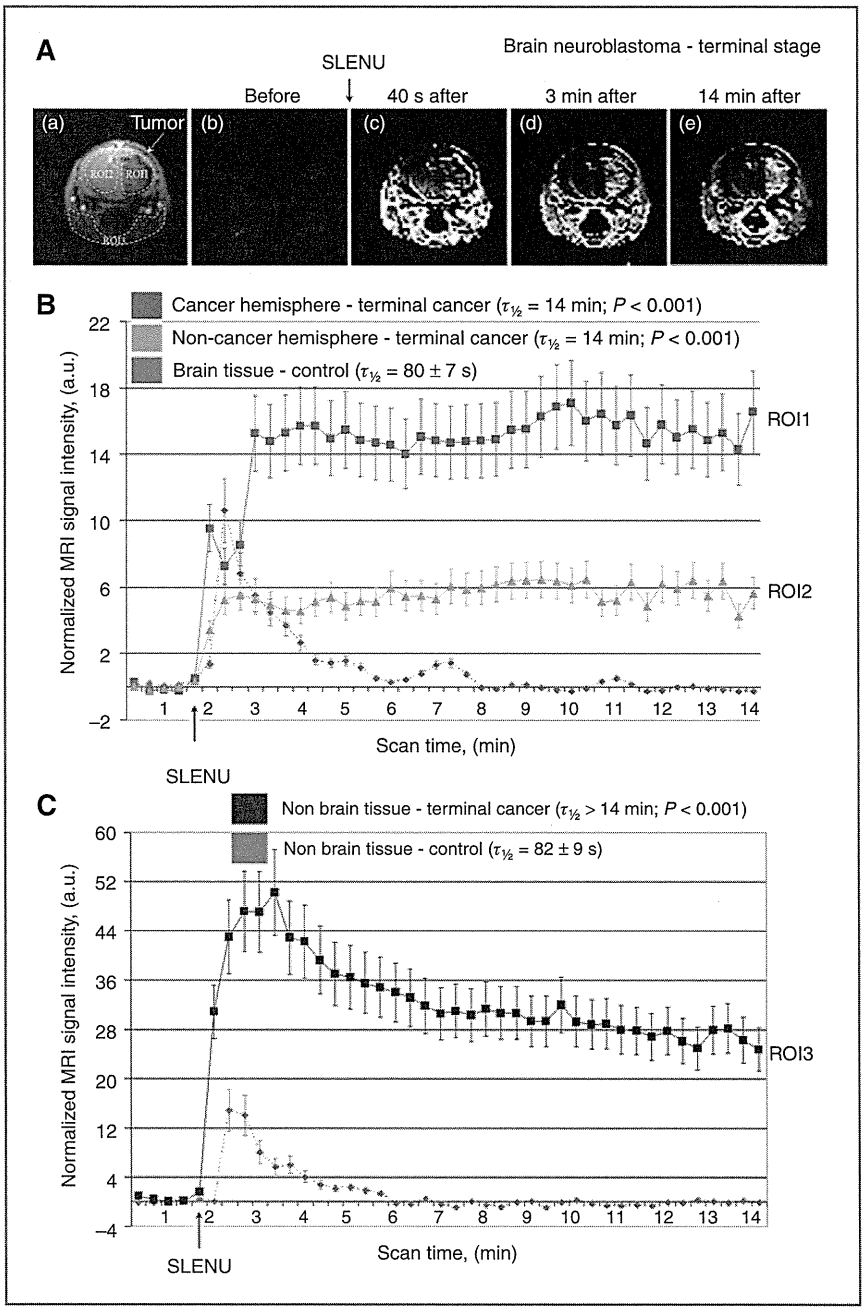


Figure 3. Healthy and neuroblastoma-bearing mice (terminal stage of cancer development). A, typical MR images of neuroblastoma-bearing brain in the terminal stage of cancer: a, MR image of mouse brain; b, extracted nitroxide-enhanced MRI signal obtained before (baseline; b) and after injection of nitroxide (SLENU; c, d, e). B and C, kinetics of the nitroxide-enhanced MRI signal in the brain, cancerous hemisphere (ROI1), and noncancerous hemisphere (ROI2; B), and surrounding (nonbrain) tissues (ROI3; C) obtained before and after injection of SLENU. Control kinetics (gray dotted lines) obtained in healthy mice are given for comparison. The data are the mean ± SD from 10 animals for each group. ROI are indicated by dotted lines on MR images. SLENU was in the oxidized (radical) form.

controls and early-stage neuroblastoma, the nitroxide-enhanced MRI signal was not detected (violet and gray curves). The kinetic measurements obtained with injection of oxidized TEMPOL are shown for comparison in Fig. 6B. The dynamics were characterized by an initial peak as a result of the accumulation of nitroxide in the brain. For healthy mice or mice with early neuroblastoma, the signal decreased rapidly to the baseline. For mice with terminal neuroblastoma, the signal remained high in both hemispheres.

The results suggest that the noncontrast reduced nitroxide was converted to its contrast-enhancing oxidized form only by the tissues of the neuroblastoma-bearing mice in the terminal stage of cancer. This experimental design proves

Published OnlineFirst March 26, 2013; DOI: 10.1158/1078-0432.CCR-12-3726



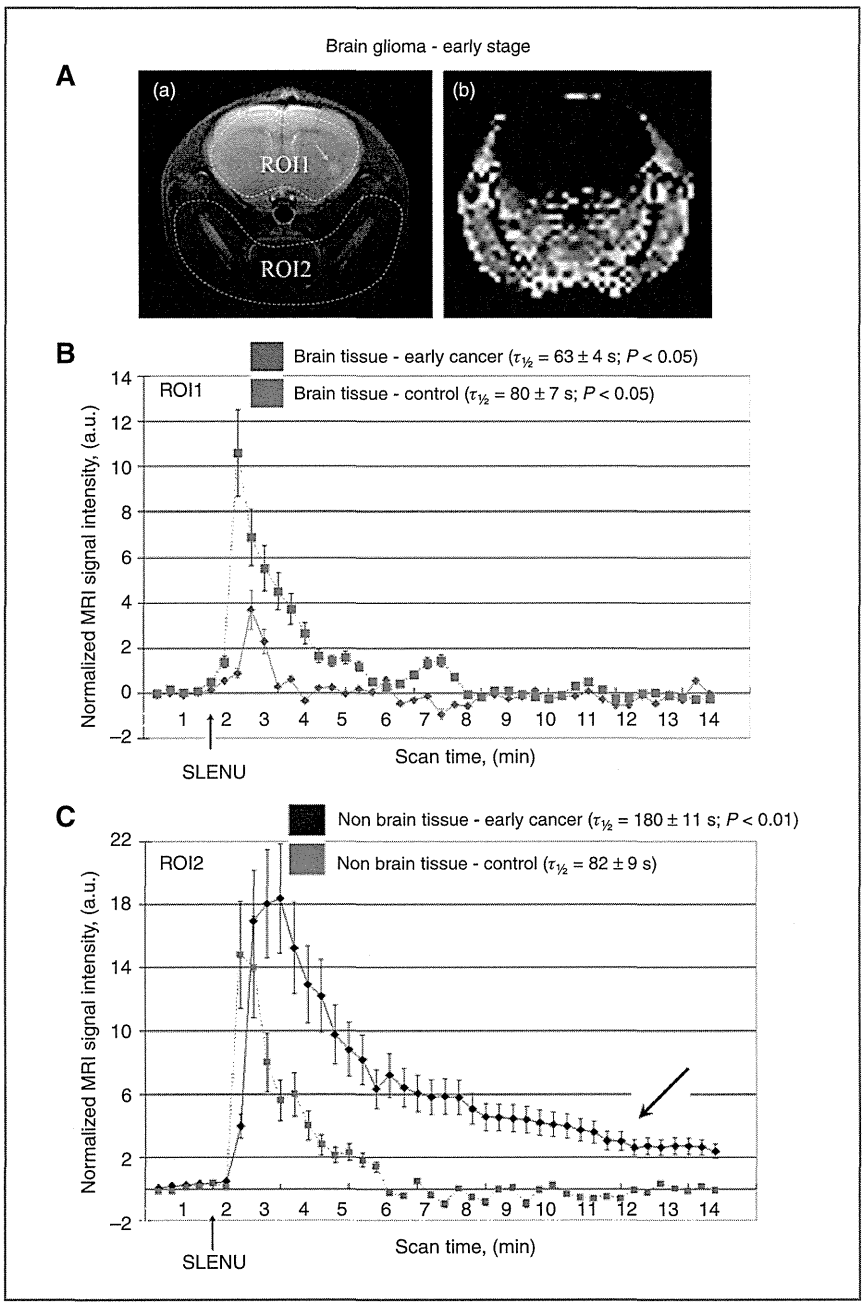


Figure 4. Healthy and glioma-bearing mice (early stage of cancer development). A, typical MR image of glioma-bearing mouse brain in the early stage of cancer: a, MR image of mouse brain; b, extracted nitroxide-enhanced MRI signal obtained 3 minutes after injection of nitroxide (SLENU). B and C, kinetics of the nitroxide-enhanced MRI signal in the brain (ROI1; B) and surrounding (nonbrain) tissues (ROI2; C) obtained before and after injection of SLENU. Control kinetics (gray dotted lines) obtained in healthy mice are given for comparison. The data are the mean ± SD from 10 animals for the control group and 5 animals for the glioma-bearing group. ROIs are indicated by dotted lines on the MR image. SLENU was in the oxidized (*radical*) form.

that these tissues are characterized by high-oxidative activity, which is not typical for tissues of healthy mice or neuroblastoma-bearing mice in the early stage of cancer.

Similar data were obtained *in vitro* using tissue specimens (brain, liver, and lung) and EPR spectroscopy (Fig. 6C). The tissues were isolated from healthy or neuroblastoma-bearing mice in the early or terminal stage of cancer. A reduced noncontrast nitroxide was added to each sample, and the appearance of the EPR spectra was detected after 10 minutes of incubation at room temperature. The appearance of EPR spectra is a result of the conversion of nitroxide probe from the reduced to oxidized (radical) form and is indicative of high-oxidative activity of the respective tissue. The EPR triplet appeared in all tissues of neuroblastoma-bearing

Published OnlineFirst March 26, 2013; DOI: 10.1158/1078-0432.CCR-12-3726



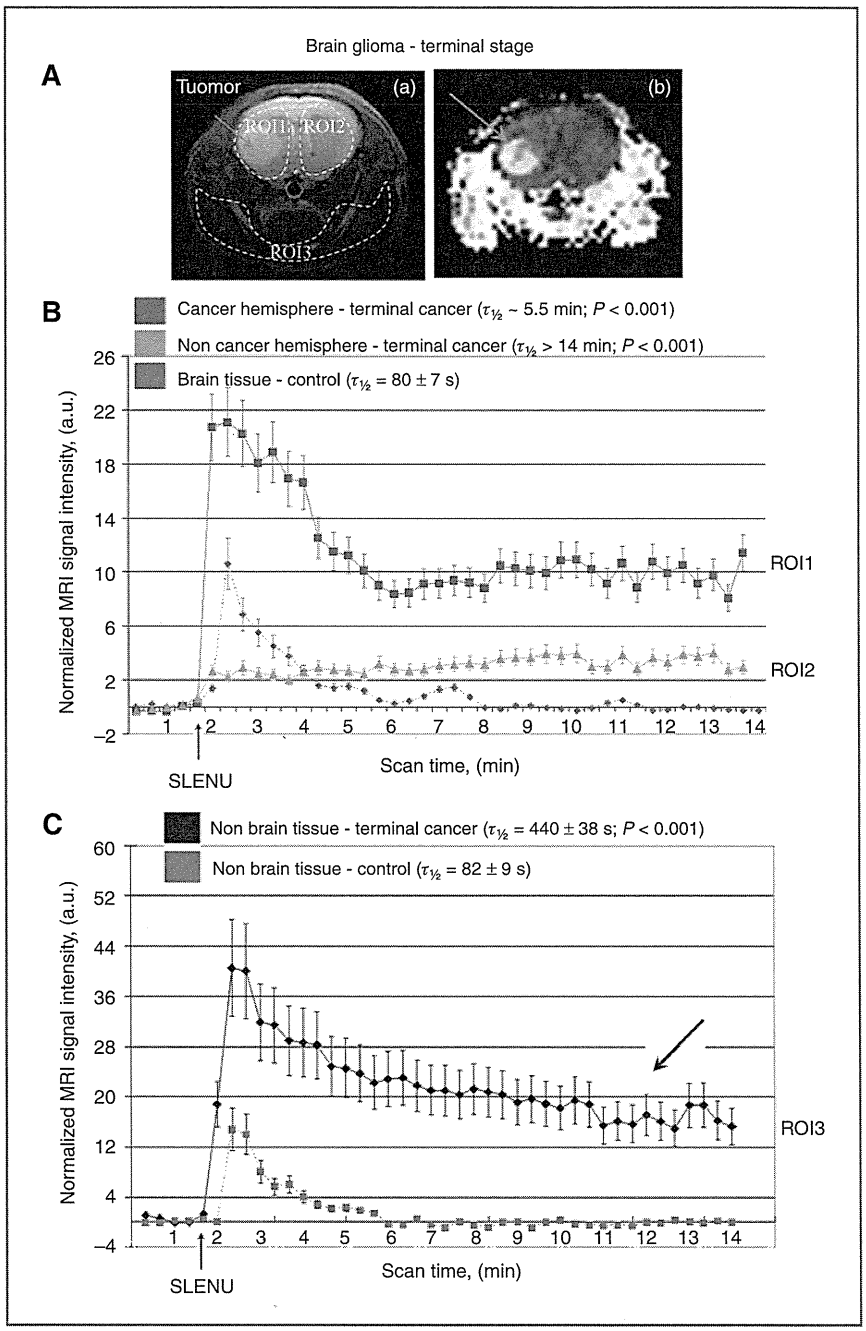


Figure 5. Healthy and glioma-bearing mice (terminal stage of cancer development). A, typical MR image of glioma-bearing mouse brain in the terminal stage of cancer: a, MR image of mouse brain; b, extracted nitroxide-enhanced MRI signal obtained 3 minutes after injection of nitroxide (SLENU). B and C, kinetics of the nitroxide-enhanced MRI signal in the brain, cancerous hemisphere (ROI1), and noncancerous hemisphere (ROI2; B), and surrounding (nonbrain) tissues (ROI3; C) obtained before and after injection of SLENU. Control kinetics (gray dotted lines) obtained in healthy mice are given for comparison. The data are the mean ± SD from 10 animals for the control group and 7 animals for the glioma-bearing group. ROIs are indicated by dotted lines on the MR image. SLENU was in the oxidized (radical) form.

mice in the terminal stage of cancer and in the liver of neuroblastoma-bearing mice in the early stage of cancer. This result indicates that all of these tissues are characterized by high-oxidative activity for the nitroxide probe. The cancerous hemisphere was characterized by the highest tissue-oxidative capacity.

### Total antioxidant capacity of brain tissue and plasma levels of matrix metalloproteinases

To investigate the potential molecular mechanism(s) of redox imbalance in cancer-bearing mice, we analyzed 2 biochemical parameters: (i) the TAC of brain tissue and (ii) the plasma levels of the MMPs, MMP2 and MMP9.

Published OnlineFirst March 26, 2013; DOI: 10.1158/1078-0432.CCR-12-3726



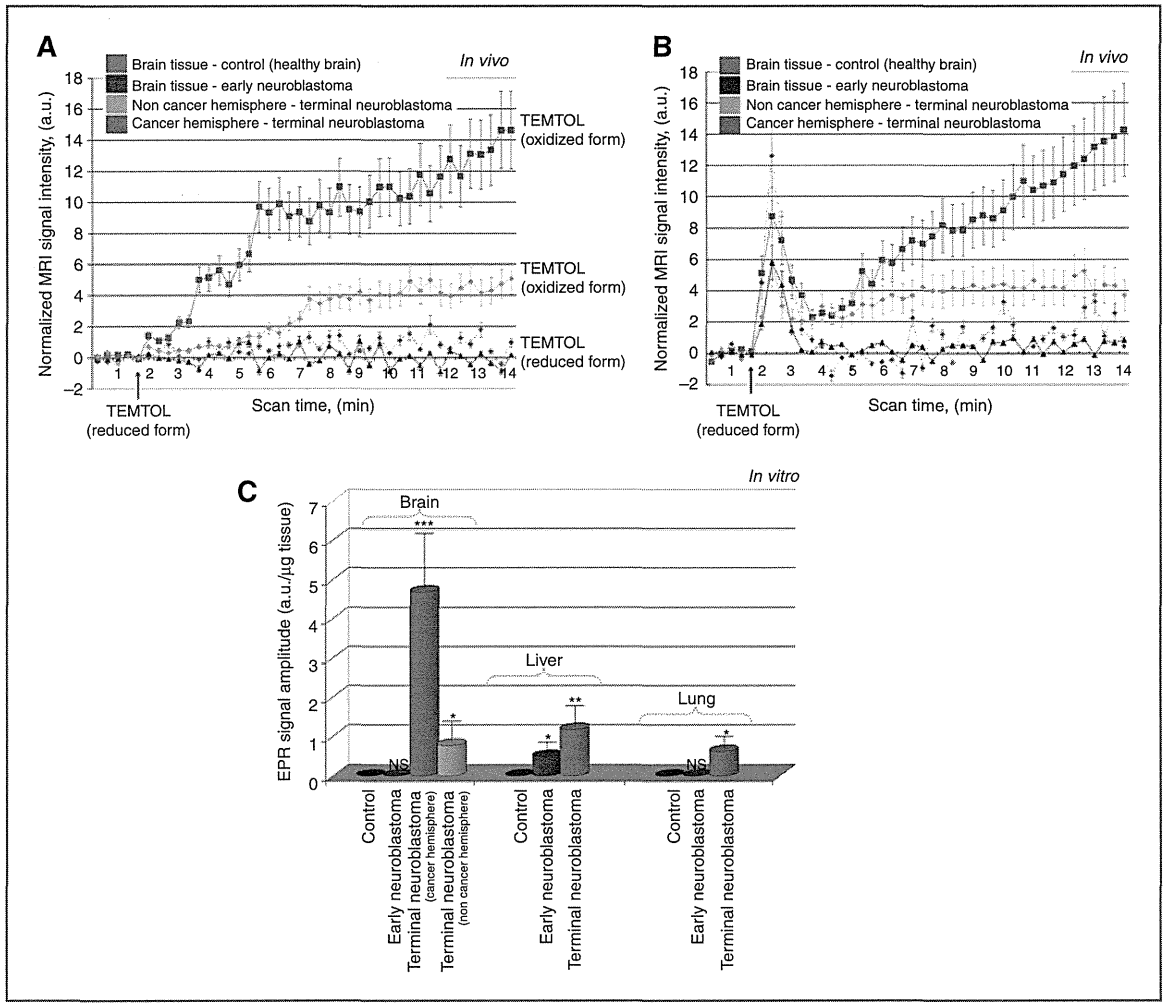


Figure 6. Analysis of the tissue oxidizing capacity *in vivo* and *in vitro* in healthy and neuroblastoma-bearing mice in the early and terminal stage of cancer. A, kinetics of the nitroxide-enhanced MRI signal in the brain before and after injection of reduced nitroxide (TEMPOL). The data are the mean ± SD from 4 animals for each group. B, kinetics of the nitroxide-enhanced MRI signal in the brain before and after injection of oxidized nitroxide (TEMPOL). The data are the mean ± SD from 6 animals for the control group and 4 animals for all other groups. C, amplitude of the EPR signal in isolated tissue specimens after addition of reduced TEMPOL. The data are the mean ± SD from 4 animals for each group. *, $P < 0.05$; **, $P < 0.01$; ***, $P < 0.001$.

It was established that the TAC of brain tissue slightly increased (~20%) in the early stage of cancer, whereas in the terminal stage, it markedly decreased (~40%) in comparison with the control (Fig. 7A). The plasma total MMP2 and MMP9 levels were significantly higher in neuroblastoma-bearing mice in the terminal stage of cancer than those in healthy mice (Fig. 7B). The plasma MMP9, but not MMP2, level also increased in neuroblastoma-bearing mice in the early stage of cancer.

## Discussion

The data show 2 important trends in carcinogenesis: (i) the tissues of cancer-bearing mammals (cancerous and noncancerous, including areas distant from the primary tumor locus) are characterized by high-oxidative activity, whereas the tissues of a healthy organism are characterized by high-reducing activity for the nitroxide and (ii) the tissue redox balance is very sensitive to the progression of cancer: in the early stage, reduction dominates over oxidation, whereas in the terminal stage, oxidation dominates over reduction. Our additional experiments on colon cancer-grafted mice treated with camptothecin within 3 weeks showed a suppression of tumor growth and significant normalization of tissue reducing potential compared with the placebo group (data to be published elsewhere).

Similar results have been reported by Matsumoto and colleagues and Hyodo and colleagues (22, 23). The authors have investigated the dynamics of the nitroxide-enhanced